Journal of Sustainability Science and Management
Volume 14 *Number* 4, August 2019: 191-200

ISSN: 1823-8556

CFD ANALYSIS ON COURSE STABILITY OF A TOWED SHIPPING CALM WATER

AHMAD FITRIADHY*, NUR ADLINA ALDIN AND NURUL AQILAH MANSOR

School of Ocean Engineering, Universiti Malaysia Terengganu, Kuala Nerus, Terengganu, Malaysia.

**Corresponding author: a.fitriadhy@umt.edu.my*

Abstract: Instability in a towed ship poses a huge accident risk while being manoeuvred on a congested waterway, which may cause the vessel to collide with other ships and structures at sea. Thus, an investigation is required to analyse course stability of a towed ship in calm waters using Computational Fluid Dynamics (CFD) simulation. A barge (1B), serving as the model of a towed ship, was employed in the simulation. Several parameters, such as towline length and towing velocity with respect to length of barge, were considered. The results revealed that increasing towline length would reduce the barge's course stability due to increment of her lateral motion. However, a longer towline length could also reduce the towline tension by 29%. The increment in towing velocity from = 0.509 m/s to 0.7276 m/s degraded the course stability of the barge as the yaw motion was increased by 41.76 %. Meanwhile, the slewing period decreased by 35.71 % as velocity increased.

Keywords: CFD, course stability, Towline tension, tug's velocity.

Introduction

Ship towing is an operation to transfer or assist unpropelled and disabled vessels. An operation that is not conducted properly causes the vessel to become instable, which may lead to accidents and result in loss of life and property. Maimun *et al.* (2011) stated that the towed vessel should be allocated a safe distance to stop and turn to avoid collision, ramming and grounding. This requires investigations in course stability to observe the behavior of towed vessels during an operation.

Most researchers reported their studies using a typical towline configuration — the symmetrical bridle towline of a towed barge. Lee (1989) presented numerical analysis on course stability of two barges; with skegs and without skegs, as well as effects of towline stiffness to the system. Fitriadhy and Yasukawa (2011) advanced the research by analysing the effects of towline length and towpoint location, while Koh and Yasukawa (2012) analysed the course stability of a barge in different depths of calm water (shallow, medium shallow and deep). Theoretical approaches were conducted by Varyani *et al.* (2005), Fitriadhy *et al.* (2013) and Sinibaldi and Bulian (2014) on course stability of a towed barge in steady winds. Fang and Ju (2009) investigated a towed barge's stability in different wave heights and wind headings using time domain simulation, while Kume *et al.* (2006) and Zan *et al.* (2012) conducted model tests on course stability of a tanker and barge, respectively. A reliable simulation is required to predict the course stability of a barge during towing operations because using a theoretical approach is impractical, expensive and time consuming. Thus, this study used the FLOW-3D software to perform computational fluid dynamics (CFD) simulation to predict the effects of a symmetrical bridle towline model on course stability of a towed barge (1B).

Materials and Methods

Governing equation

The CFD flow solver in FLOW-3D Version 10.1 is based on the incompressible unsteady Reynolds-Averaged Navier Stokes equation (RANSE), in which the solver applies the Volume of Fluid (VOF) to track free surface elevation. The interface between fluid and solid boundaries is simulated with the fractional area volume obstacle representation favour method.

This method computes open area and volume in each cell to define the area that is occupied by an obstacle.

Continuity and Momentum Equation

The continuity and momentum equations for a moving object and the relative transport equation for VOF function were stated in Equations 1, 2 and 3.

$$\frac{V_f}{\rho}\frac{\partial \rho}{\partial t} + \frac{1}{\rho}\nabla \cdot \left(\rho \vec{u} A_f\right) = -\frac{\partial V_f}{\partial t} \quad (1)$$

$$\frac{\partial \vec{u}}{\partial t} + \frac{1}{V_f}\left(\vec{u} A_f \cdot \nabla \vec{u}\right) = -\frac{1}{\rho}\left[\nabla \rho + \nabla \cdot \left(\tau A_f\right)\right] + \vec{G} \quad (2)$$

$$\frac{\partial F}{\partial t} + \frac{1}{V_f}\nabla.\left(F \vec{u} A_f\right) = -\frac{F}{V_f}\frac{\partial V_f}{\partial t} \quad (3)$$

where is the density of the fluid, is the fluid velocity, is the volume fraction, is the area fraction, is the pressure, is the viscous stress tensor, denotes gravity and is the fluid fraction.

In the case of coupled GMO's motion, equations 1 and 2 were solved at each time step and the location of all moving objects was recordedand the area and volume fractions updated using the FAVOR technique. Equation 3 was solved with the source term $\left(-\frac{\partial V_f}{\partial t}\right)$ on the right-hand side, which was computed as in equation 4.

$$-\frac{\partial V_f}{\partial t} = \vec{U}_{obj} . \vec{n} S_{obj} / V_{cell} \quad (4)$$

where, is the surface area, surface normal vector, $_{obj}$ is the velocity of the moving object at a mesh cell and is the total volume of the cell (FLOW-3D 10.1.1 User Manual, 2013).

Turbulence Model

The two-equation () model calculates turbulent kinetic energy (k) and dissipation rate (ε) to find the turbulent mixing length (L_T) dynamically. The transport equation for included the convection and diffusion of the turbulent kinetic energy, production of turbulent kinetic energy due to shearing and buoyancy effectsand diffusion and dissipation due to viscous loss within the turbulent eddies. Buoyancy production only occurred if there was a non-uniform density in the flowand that included the effects of gravity and non-inertial accelerations. The transport equation is stated in equation 5.

$$\frac{\partial k_T}{\partial t} + \frac{1}{V_F}\left\{uA_x\frac{\partial k_T}{\partial x} + vA_y\frac{\partial k_T}{\partial y} + wA_z\frac{\partial k_T}{\partial z}\right\} = P_T + G_T + Diff_{k_T} - \varepsilon_T \quad (5)$$

where are FLOW-3D's FAVOR™ functions, is the turbulent kinetic energy production according to equation 6.

$$P_T = CSPRO\left(\frac{\mu}{\rho V_F}\right) \times \left\{ \begin{array}{c} 2A_x\left(\frac{\partial u}{\partial x}\right)^2 + 2A_y\left(R\frac{\partial v}{\partial y}\xi\frac{u}{x}\right)^2 + 2A_z\left(\frac{\partial w}{\partial z}\right)^2 \\ + \left(\frac{\partial v}{\partial x} + R\frac{\partial \mu}{\partial y} + \xi\frac{v}{x}\right)\left[A_x\frac{\partial v}{\partial x} + A_y\left(R\frac{\partial u}{\partial y} + \xi\frac{v}{x}\right)\right] \\ + \left(\frac{\partial u}{\partial z} + \frac{\partial w}{\partial x}\right)\left(A_z\frac{\partial u}{\partial z} + A_x\left(R\frac{\partial w}{\partial x}\right)\right) \\ + \left(\frac{\partial v}{\partial z} + R\frac{\partial w}{\partial y}\right)\left(A_z\frac{\partial v}{\partial z} + A_y R\frac{\partial w}{\partial y}\right) \end{array} \right\} \quad (6)$$

where CSPRO is a turbulence parameter.

In the case of this computation for turbulent condition, the model was proposed, where and were turbulent kinetic and turbulent dissipation energies, respectively. Twotransport equations for the turbulent kinetic energy and its dissipation in the so-called " model» were used in the computational simulation. It was reasonable since this equation model provided more reliable approximations to many types of flows (FLOW-3D 10.1.1 User Manual, 2013). In addition, the model was quite economical in terms of CPU time, compared to, for example, the SST turbulence model, which increased the required CPU time by nearly 25 %. Talaat *et al*. (2017) stated that the model could decrease computational time and resources by reducing the number of nodes in the near wall regions, which allowed for more probing simulation and trial geometries.

Body Motion Computation

The body motion was analysed in a space-fixed Cartesian coordinate system, the global coordinate system. The governing equation of the six degree of freedom (DOF) of a rigid body motion can be expressed in this coordinate system as equations 7 and 8.

$$\frac{d}{dt}(m\vec{v}_C) = \vec{f} \quad (7)$$

$$\frac{d}{dt}(M_C.\vec{\omega}_C) = \vec{m}_C \quad (8)$$

The index C denoted the centre mass of the body, *m* denoted the mass of the body, was the velocity vector, was the tensor of the moments of inertia, $_c$ was the angular velocity vector, denoted the resulting force vectorand $_c$ denoted the resultant moment vector acting on the body (Wu *et al.*, 2011). The resultant force had three components; surface force, field forces and external forces:

$$\vec{f} = \int_S (T - \rho I).\vec{n}dS + \int_V \rho_b \vec{b}dV + \vec{f}E \quad (9)$$

Here, is the density of the body. The only field force considered was gravity, so the volume integral of above equation (right hand side) would reduce to , where was the gravity acceleration vector. The vector denoted the external forces acting in the body (Yan & Huang, 1996).

Simulation Conditions

Principal Data of Vessel

The principal dimensions of barge (1B) are presented in Table 1. Her respective body plan is shown in Figure 1.

Parametric Analysis

Table 2 shows various of towlines used in the simulation. Towing's velocity was kept constant at 0.509 m/s. The tug was replaced with the sphere that had similar characteristics of a tug. Various towing velocity was used in the

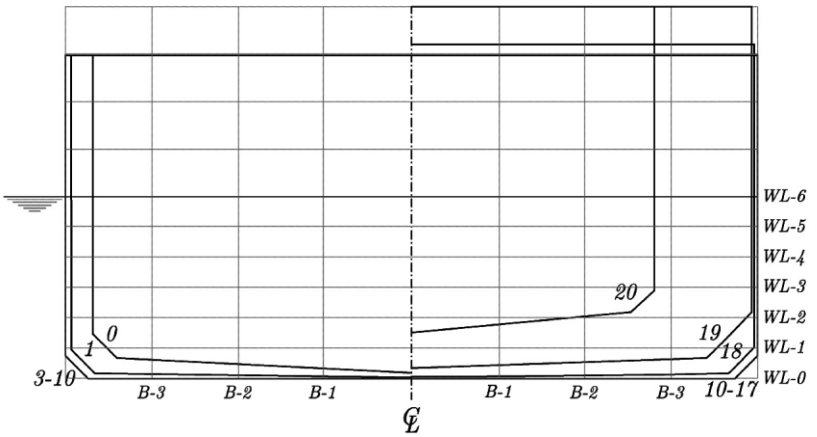

Figure 1. Barge (1B) body plan

Table 1. Principal dimensions of barge (1B)

Description	1B	
	Full-scale	Model
Length, L(m)	60.96	1.219
Breadth, B(m)	10.67	0.213
Draft, d(m)	2.74	0.0548
Volume, V()	1646.2	0.01317
L/B	5.71	5.71
Block coefficient,	0.92	0.92
k_{yy2}/L	0.3266	0.3266
$X_{(G\ abaft\ the\ midship),}(m)$	-1.04	-0.0208

simulation as shown in Table 3, with the towline length set at a constant value of =2.0.

Table 2. Various towline lengths

Towline length (ℓ')	Towing's velocity, V_s(m/s)
1.0	
2.0	0.509
3.0	

Table 3. Various towing velocities

Towline length (ℓ')	Towing's velocity, V_s(m/s)
2.0	0.5090
	0.5820
	0.6549
	0.7276

Computational Domain and Boundary Condition

The computational domain used a structured mesh that was defined in a Cartesian. Referring to Figure 2, the boundary conditions were marked in the mesh block. The condition at X-max was specified in terms of velocity so that there was flow of water. To save on computational time, a velocity of 0.509 m/s was given to the water at X-max. For X-min, Y-max and Y-min, outflow was used to prevent reflection while Z-min was specified as pressure and Z-max was symmetry. The boundary conditions for this simulation are shown in Table 4. The barge was initially in a straight-tow configuration.

The barge was coupled with a towline. The sphere model, which acted as the tow ship, was assigned a prescribed motion while the barge, as the towed ship, was set as coupled motion in X-translational, Y-translational and Z-rotational motions (surge, sway and yaw). The towline was set as a massless elastic rope with spring coefficient of 1297.6 N/m.

Based on the applications of FLOW-3D, the average duration of every simulation was about 70 to 80 hours (four parallel computations) on a HP Z820 workstation PC powered by an Intel (R) Xeon (R) CPU ES-2690 v2 @ 3.00 GHz (double processor), with of 32.0 GB RAM and 64-bit operating system.

Table 4: Boundary conditions

Boundary	Conditions	
	Mesh block 1	Mesh block 2
X_{min}	Outflow	Symmetry
X_{max}	Specified Velocity	Symmetry
Y_{min}	Outflow	Outflow
Y_{max}	Outflow	Outflow
Z_{min}	Symmetry	Symmetry
Z_{max}	Specified Pressure	Symmetry

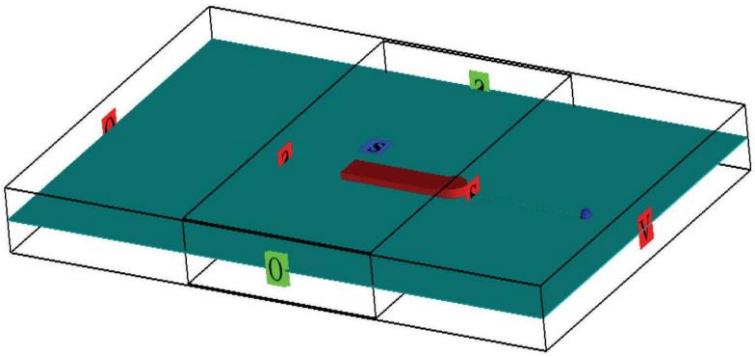

Figure 2: Boundary conditions

Mesh Independent Analysis

Mesh independent study was necessary to examine the adequate number of mesh to ensure the accuracy of computated results. Table 5 shows the results of the mesh independent study of the system with =2.0 and =0.509 in calm waters. The total number of real cells was about 3,029,103 in Case C, which was then selected from the other three cases with reasonable accuracy of CFD solution associated with less computational time.

Table 5: Mesh independent study

Case	Total number of real cells	Maximum sway motion (m)
A	2012526	1.008901
B	2504614	1.122711
C	3029103	1.129529
D	3460320	1.119115

The meshing was generated using FLOW-3D as shown in Figure 3. An extra refinement of the mesh, called the nested block, was added to increase meshing resolution. The cell sizes were 0.02 in mesh block 1 and 0.01 in mesh block 2.

Results and Discussion

Figures 6 to 9 show that the CFD simulations had been successfully carried out to predict course stability in the towing system at various towline length and velocity. The simulations results of sway and and yaw motions of the barge associated with the towline tension were discussed.

Effects of Towline Length

The characteristics of sway and yaw motion in various towline length is displayed in Figure 6. Extending the towline length from $\ell' = 1.0$ to 2.0 and 3.0 resulted in significant increments of sway motion by 35.17% and 219%, respectively. The fishtailing period of barge (1B) was lowered by 25 % as towline length increased from $\ell' = 1.0$ to 3.0. It was noted that yaw motion increased

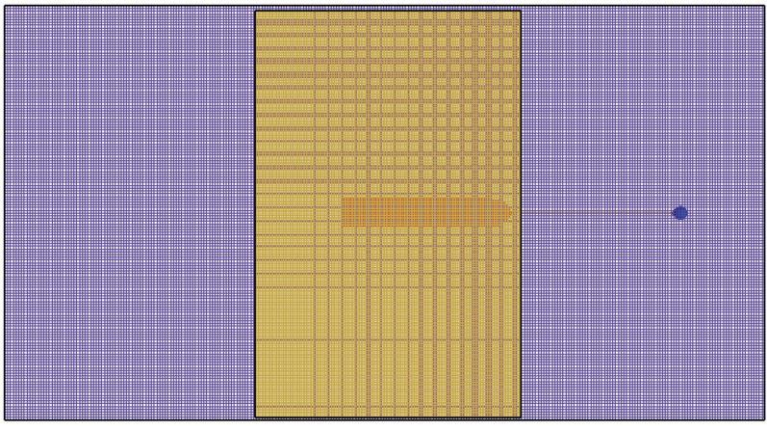

Figure 3: Meshing generation by FLOW-3D Version 10.1

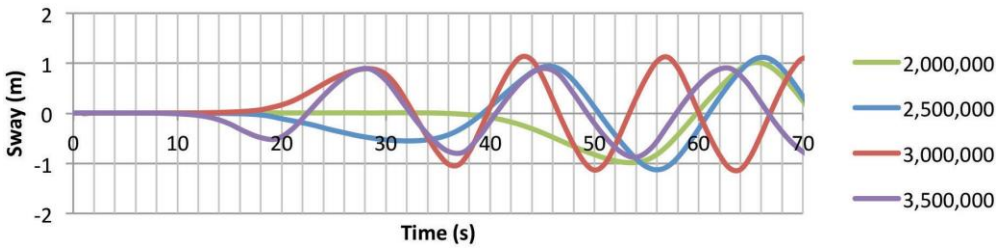

Figure 4: Mesh independent study

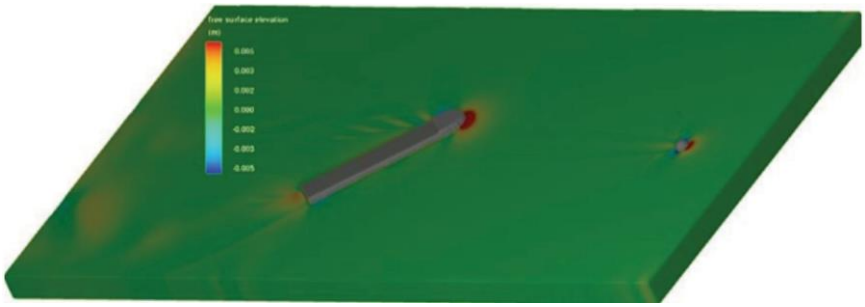

Figure 5: Example of CFD visualisation in 3D view (ℓ' = 2.0 and V_s=0.509 m/s)

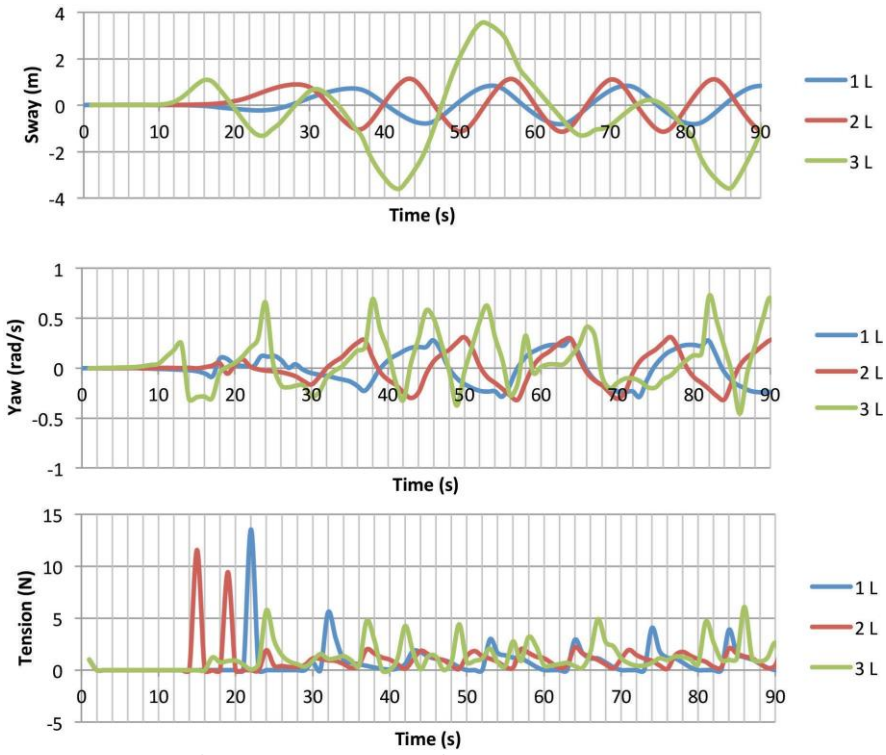

Figure 6: Characteristics of sway and yaw motion of barge 1B associated with tension at various towline lengths

by 152 % as the towline length increased from ℓ' =1.0 to 3.0. The course stability began degrading when the increasing towline length augmented the sway motion of the barge. As remarked in the numerical approach by Fitriadhy and Yasukawa (2011), the lateral motion increased as the towline length was extended from ℓ' = 1.0 to 3.0.

At the beginning of simulation, t = 0 – 30 s, fluctuation occurred due to loosening and tightening of the towline. Based on Figure 7, which shows free surface elevation, it could be observed that ℓ' = 3.0 was showing a vigorous sway motion compared to ℓ' = 1.0 and 2.0.

Effect of Towing's Velocity

Figure 8 shows the characteristics of sway and yaw motion associated with dynamic towline tension in various towing velocities. The subsequent increase of towing velocity from

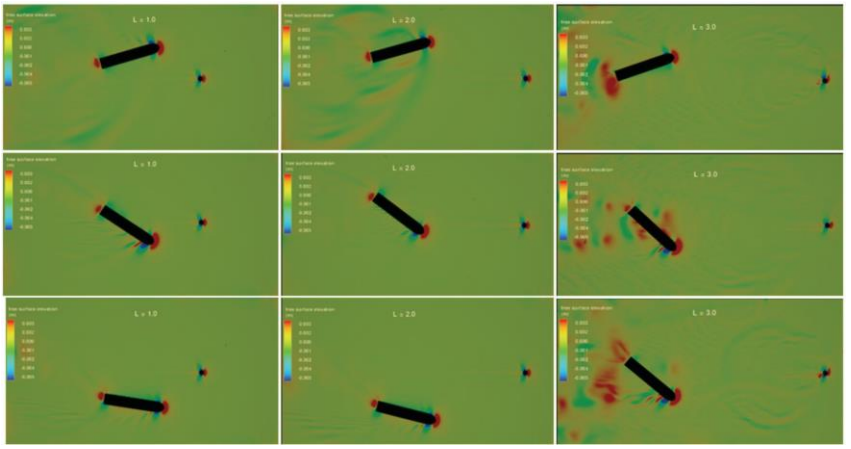

Figure 7: Free surface elevation, $\ell' = 1.0$ (left), $\ell' = 2.0$ (middle) and $\ell' = 3.0$ (right), *Vs* = 0.509 *m/s*

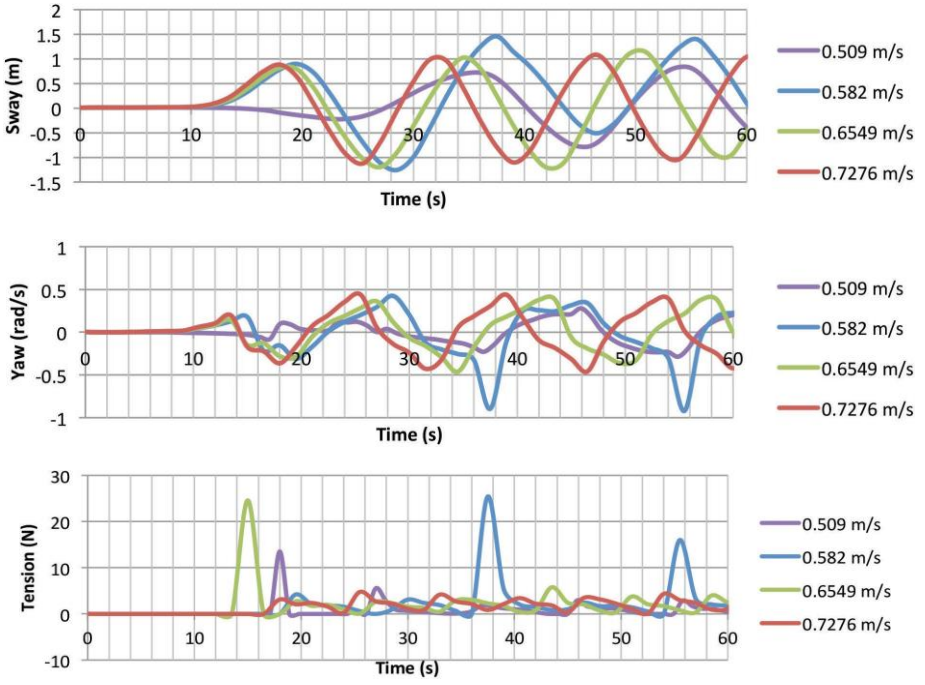

Figure 8: Characteristics of sway and yaw motion of barge 1B associated with tension at various towing velocities

0.509 m/s to 0.582 resulted in a reduction of sway motion by 28.69 %. However, the lateral motion of the barge decreased by 25.7 % when the towing velocity was increased from 0.582 m/s to 0.7276 .

The yaw motion of the barge increased by 41.76% as the speed increased from 0.509 m/s to 0.7276 . Reduction of slewing period by 35.71% resulted due to increasing towing's velocity. Higher wave crest (dark colour) present at the bow region and prone to increase as the velocity increased from 0.509 m/s to 0.7276 m/s, which was proportional to high pressure as shown in Figure 9.

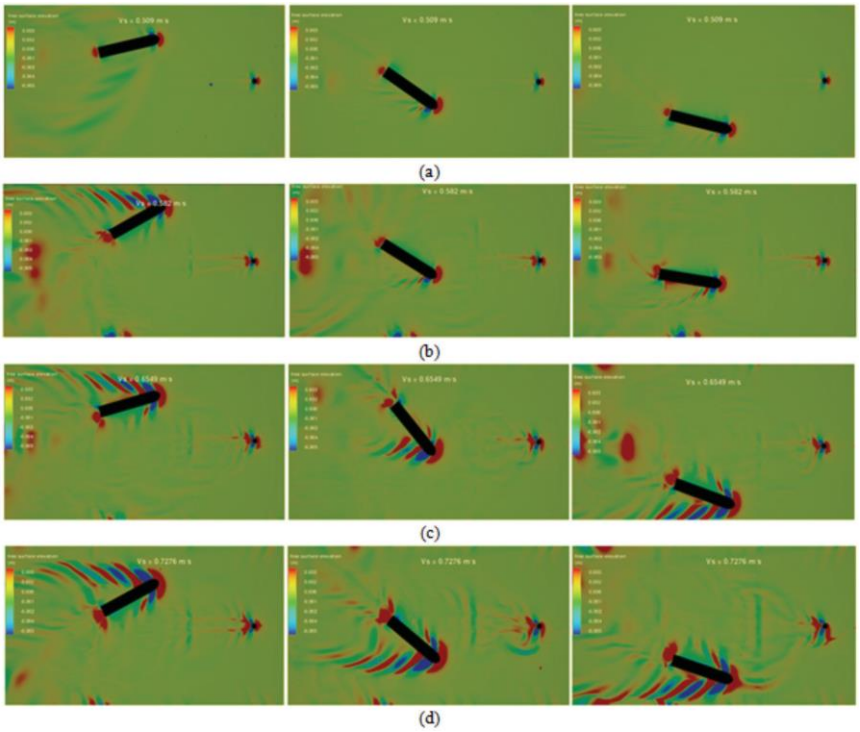

Figure 9: Free surface elevation, $\ell' = 2.0$, *Vs* = (a) 0.509, (b) 0.582, (c) 0.6549 and (d) 0.7276 *m/s*

Conclusions

The CFD analysis on course stability of a ship's towing system was successfully performed using FLOW-3D Version 10.1 software. The effects of different towline lengths and towing velocities were investigated. The simulation results were as follows: Extending towline length (from 1.0 to 3.0 would degrade course stability of the barge as indicated by an increase of sway and yaw motions. However, the slewing period decreased by 42.86 % and 14.29 % when = 1.0 and 3.0, respectively, while the towline tension had decreased by 29 %. The increase in towing velocity from 0.509 to 0.582 increased the yaw motion by 37 %, but it slightly decreased when the velocity was increased from 0.582 to 0.6549 . Meanwhile, towline tension could be reduced by 58.8 % when velocity was increased from 0.509 to 0.7276 .

Acknowledgements

The authors would like to acknowledge the financial support from Fundamental Research Grant Scheme (FRGS) Vot No. 59414 provided by the Higher Education Ministry.

References

Fang, M. C., & Ju, J. H. (2009). The dynamic simulations of the ship towing system in random waves. *Marine Technology*, *46*(2), 107-115.

Fitriadhy, A., & Yasukawa, H. (2011). Course stability of a ship towing system. *Ship Technology Research*, *58*(1), 4-23.

Fitriadhy, A., Yasukawa, H., & Koh, K. (2013). Course stability of a ship towing system in wind. *Ocean Engineering*, *64*, 135-145.

FLOW-3D 10.1.1 User Manual. (2013). Flow Science Inc.

Koh, K. K., & Yasukawa, H. (2012). Comparison study of a pusher–barge system in shallow water, medium shallow water and deep-water conditions. *Ocean Engineering, 46*, 9-17.

Kume, K., Hasegawa, J., Tsukada, Y., Fujisawa, J., Fukasawa, R., & Hinatsu, M. (2006). Measurements of hydrodynamic forces, surface pressureand wake for obliquely towed tanker model and uncertainty analysis for cfd validation. *Journal of Marine Science and Technology, 11*(2), 65-75.

Lee, M. L. (1989). Dynamic stability of nonlinear barge-towing system. *Applied Mathematical Modelling, 13*(12), 693-701.

Maimun, A., Priyanto, A., Muhammad, A., Scully, C.and Awal, Z. (2011). Manoeuvring prediction of pusher barge in deep and shallow water. *Ocean Engineering, 38*(11), 1291-1299.

Sinibaldi, M., & Bulian, G. (2014). Towing simulation in wind through a Nonlinear 4-DOF Model: Bifurcation analysis and occurrence of fishtailing. *Ocean Engineering, 88*, 366-392.

Talaat, W. M., Hafez, K., & Banawan, A. (2017). A CFDpresentation and visualization for a new model that uses interceptors to harness hydro-energy at the wash of fast boats. *Ocean Engineering, 130*, 542-556.

Varyani, K. S., Barltrop, N. D., & Pham, X. P. (2005). Fishtailing Instabilities in Emergency Towing of Disabled Tankers. *Paper presented at the The Fifteenth International Offshore and Polar Engineering Conference*.

Wu, C.-S., Zhou, D. C., Gao, L., & Miao, Q. M. (2011). CFD computation of ship motions and added resistance for a high-speed trimaran in regular head waves. *International Journal of Naval Architecture and Ocean Engineering, 3*(1), 105-110.

Yan, S., & Huang, G. (1996). Dynamic performance of towing system-simulation and model experiment. *Proceedings, OCEAN, 96*.

Zan, U. I., Yasukawa, H., Koh, K. K., & Fitriadhy, A. (2012). Model experimental study of a towed ship's motion. *The 6th Asia-Pacific Workshop on Marine Hydrodymics-APHydro*.